

APPARATUS AND DEMONSTRATION NOTES

Jeffrey S. Dunham, *Editor*

Department of Physics, Middlebury College, Middlebury, Vermont 05753

This department welcomes brief communications reporting new demonstrations, laboratory equipment, techniques, or materials of interest to teachers of physics. Notes on new applications of older apparatus, measurements supplementing data supplied by manufacturers, information which, while not new, is not generally known, procurement information, and news about apparatus under development may be suitable for publication in this section. Neither the *American Journal of Physics* nor the Editors assume responsibility for the correctness of the information presented. Submit materials to Jeffrey S. Dunham, *Editor*.

Investigating vortex streets behind real and virtual bluff bodies

Y. D. Afanasyev^{a)} and C. G. Deacon

Department of Physics and Physical Oceanography, Memorial University of Newfoundland, St. John's, Newfoundland, Canada A1B 3X7

(Received 4 July 2005; accepted 6 January 2006)

This paper describes a laboratory experiment designed to study regular arrays of vortices occurring behind an object in a stream of fluid. This phenomenon is observed in industrial flows, flows in the ocean, and in the atmosphere. In the first part of the experiment we consider the flow behind a circular cylinder. In the second part of the experiment the effect of a body on the fluid is imitated by using an appropriate force field, with no real body present in the fluid. The force field (virtual body) is created by a permanent magnet located above the surface of water in combination with an electric current applied in the horizontal direction. The apparatus required for the experiment is inexpensive and easy to construct. © 2006 American Association of Physics Teachers.

[DOI: 10.1119/1.2173274]

I. INTRODUCTION

The phenomenon of regular vortex shedding behind bodies in a stream of fluid is often observed in nature.^{1,2} For example, vortex streets can be observed on a large scale in satellite images of cloud cover behind mountainous islands. On a smaller scale, the flutter of a flag in the wind or the generation of sound by a wire are all related phenomena.

We consider the classical fluid mechanics problem of flow behind a circular cylinder. This problem has been the subject of serious investigation for over a hundred years.³ The underlying (nonlinear) phenomena which cause instability in the form of vortex shedding are quite complex; however, the vortex street itself is simple, highly periodic, and robust. The characteristics of these flows can be measured easily and analyzed using dimensional analysis. A body in a stream experiences a drag force; therefore, the effect of the body on the fluid is described by the force equal to the drag force in magnitude and acting in the opposite direction. We can create a “virtual” body by imitating this force, with no real body present in the fluid. An electromagnetic method is used for this purpose.

The goal of this paper is to describe a simple, low-cost experiment for the advanced undergraduate laboratory and to introduce students to methods of dimensional analysis. While the experiment is simple enough to be performed by undergraduates, it exposes students to the kinds of methods that are encountered often in advanced research.

II. EXPERIMENT

The apparatus is illustrated schematically in Fig. 1. The flows are generated in a Plexiglas tank that is 50 cm long, 10 cm deep, and 20 cm wide. The tank contains two layers of salt water, each of depth 0.5 cm, but of differing salt concentration, the lower layer being more dense than the upper one. Two layers are used to minimize the vertical component of velocity, thus constraining the flow to two dimensions.⁴ Two copper pipes at the side walls of the tank serve as electrodes,⁵ and, a rare-earth permanent magnet of diameter $d=0.5$ cm is located approximately 0.1–0.3 cm above the liquid surface. The interaction of the magnetic field (typically 0.04–0.09 T in the vertical direction) with the electric current of magnitude $j=0-3$ A results in a horizontal force exerted locally on the fluid in the direction perpendicular to the electric current. Charged particles (ions in dissociated electrolyte solution) drift toward the electrodes: positive ions move towards the cathode while negative ions move towards the anode. The Lorentz force, $\mathbf{F}=q\mathbf{v}\times\mathbf{B}$, is perpendicular to both the magnetic field and the current. Because the oppositely charged particles move in opposite directions, the resulting force is in the *same* direction in the horizontal plane for positive and negative ions. If, on the other hand, the particles, in addition to drift, are carried by the fluid motion, the total force due to this additional velocity component is zero, since positive and negative particles move in the same direction and their total charge is zero. Hence, the electromagnetic force on the fluid does not depend on the motion of the fluid. The force is applied locally to the fluid in a volume

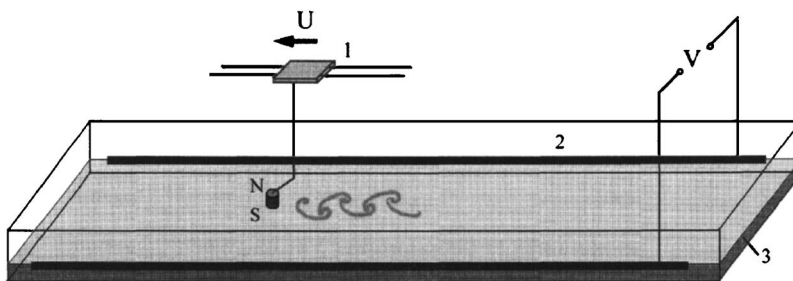


Fig. 1. Sketch of the experimental setup: (1) translation stage with a magnet attached, (2) electrodes, (3) two-layer fluid.

in which the vertical component of magnetic field is significant. The horizontal extent of this area is of the order of the magnet diameter. The magnetic field decreases rapidly (approximately as z^{-3}) in the vertical direction, hence the magnet effectively induces motion of the fluid in the upper layer only.

The magnet is translated along the tank by a stepping motor on a translation stage. The translation stage was constructed from a modified carriage assembly that was obtained from an old inkjet printer. A simple controller for the stepping motor was designed to allow the translation velocity, U , to be varied in the range $U=0.2-5$ cm/s. The translation stage was leveled to ensure that the distance between the magnet and the surface of water did not change as the magnet was moved along the tank. The polarity of the magnet and the direction of the current were chosen so that the resulting force was applied on the fluid in the same direction as that of the translation of the magnet. This imitates the force applied by a towed body on the fluid (a reaction to the drag force).

A PC video camera placed above the tank is used to record video sequences or single snapshots of the flow. A camera with adjustable optics and with software for reducing the horizontal distortions (most cameras have a wide-angle objective lens) is preferred for this purpose. Most cameras provide VGA resolution (640×480 pixels) and frame rates up to 30 fps, which is quite sufficient for the purpose of this experiment. The recorded video can then be analyzed frame by frame using the standard software that is usually supplied with such a camera. The flow is illuminated by a fluorescent lamp placed below the tank. A food dye can be used to visualize the flows. Several drops of dyed fluid are injected by a pipette along the axis of motion of the object before the object is towed; the dyed fluid is prepared from equal parts of lower and upper layer so that the particles remain at the interface between the layers and form clearly visible patterns of the flow. Unfortunately, the dye eventually contaminates the fluid. An alternate method is to use a pH-indicator such as thymol-blue. The color of this indicator solution is orange-yellow in its neutral state and deep-blue in the basic state. We use a basic solution of the indicator instead of a dye. The water in the upper layer is made slightly acidic, so that it takes only a few minutes after the experiment for the injected blue fluid to become yellow again due to diffusive chemical reaction.

An outline of the steps involved in the experiment follows.

A. Density stratification

The tank is filled with two layers of salt water each of depth 0.5 cm. The concentration of salt is 30 and 250 g/l in

the upper and lower layers, respectively. To prepare a two-layer system without mixing the fluids, the heavier layer is first poured into the tank and a sheet of paper is floated on top of it. The less dense fluid is then carefully poured onto the sheet, and the latter is then (very carefully) removed. Another method is to pour the less dense fluid into the tank first, and the heavier fluid can be delivered through a thin tube placed (not too tight) against the bottom of the tank to allow the fluid to spread slowly along the bottom. This second method allows for a very sharp interface between the layers, but is somewhat more time consuming to achieve. The two-layer stratification is very stable due to the large density difference between the layers; however, it changes with time due to diffusion of the salt. The stratification can be used for approximately 1 hour; after this it must be replaced.

B. Circular cylinder

The first set of experiments is performed with circular cylinders of differing diameters up to 1 cm. No electric current is needed for these experiments. A cylinder is placed vertically in a holder so that the distance between the lower end of the cylinder and the bottom of the tank does not exceed 0.1–0.2 cm. By increasing the speed of translation of the cylinder, a transition from the stable regime to a regime with periodic vortex shedding (Kármán-Bénard vortex street) can be observed. A typical view of the vortex street is shown in Fig. 2. The period of vortex shedding can be measured from a video sequence, which allows us to determine the time between the events when a vortex of one sign is shed. Alternatively, the wavelength of the vortex street can be measured from a snapshot of the flow as the distance between vortices of one sign.

C. Calibration

In the experiments with the magnet it is impossible to determine the exact value of the force acting in the fluid without exact knowledge of the drift velocities of ions; however, an indirect method can be used to obtain the value of this important control parameter. The magnitude of the force



Fig. 2. Kármán-Bénard vortex street behind a circular cylinder of diameter $d=0.478$ cm moving with velocity $U=1.74$ cm/s with $Re=83$.

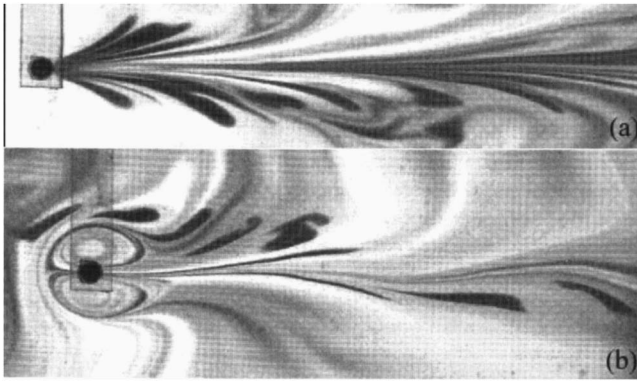


Fig. 3. Images of the flow generated by a magnet (virtual body) for different regimes: (a) stable jet and (b) vortex dipole with a wake behind it. Experimental parameters: (a) $U=1.45$ cm/s, $J=0.8$ cm³/s² and (b) $U=0.29$ cm/s, $J=0.7$ cm³/s².

is controlled in the experiments by varying the current that passes between the two copper pipes. If the magnet is stationary, the localized force generates a starting vortex dipole, which is a jet with a pair of vortices of opposite sign at its front. Previous studies⁶ show that the distance D traveled by a dipole varies with time t as

$$D(t) = (3J/4\pi)^{1/3} t^{2/3}, \quad (1)$$

where J is the force (linear momentum flux) exerted by the magnet per unit mass and per unit depth of the fluid. The dimensions of J are $[J]=L^3/T^2$ where L and T represent the units of length and time. The distance D is measured from the origin (the center of the magnet) to the front of the vortex dipole. The magnet is located approximately at the center of the tank for this calibration. We also assume that the flow is approximately uniform in the vertical direction along the depth of the layer. A drop of dyed fluid is injected under the magnet before the start of the experiment. Individual frames from the recorded video of the flow can be saved and analyzed using a standard image tool in MS Windows. The position of the cursor in pixels is used to measure the length D at different frames, and a centimeter scale placed under the tank prior to recording the video enables D to be calculated in centimeters. Knowing the video frame rate, the time between successive frames can be determined.

Equation (1) allows us to relate the force J to the magnitude of the electric current. D is measured as a function of time for different values of current j . The power-law ($t^{2/3}$)

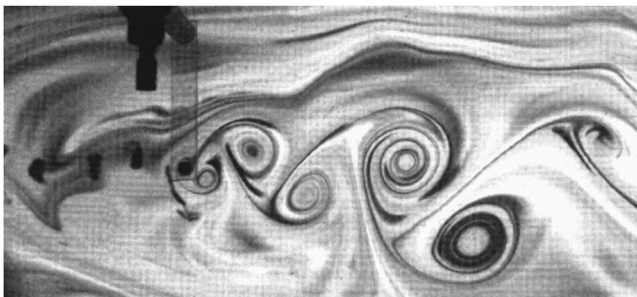


Fig. 4. Sequence of video frames showing different phases of a regular vortex shedding regime for experimental parameters $U=0.58$ cm/s and $J=4.25$ cm³/s².

dependence is confirmed for each run and the momentum flux, J , is estimated from the slope of the D versus $t^{2/3}$ graph. The calculated values of J can be plotted against current j to obtain a linear relation of the form $J=\beta j$, where the coefficient β depends on the particular parameters of the apparatus, namely the distance of the magnet from the surface of water, the magnetization of the magnet, the area of the electrodes, and the stratification. In the present work the value of β was in the range 0.3–1.5 for J measured in cm³/s² and j in A. After calibrating, the magnet and the electrodes cannot be adjusted. The calibration procedure should be repeated two or three times between successive experiments because the value of the coefficient β changes slowly with time due to changes in the stratification.

An alternative method to measure the force applied on the fluid requires measurements of velocities in the fluid using a particle image velocimetry (PIV) system such as that described in Ref. 7. The force can then be obtained by integration along a contour around the origin using a flux formula given in Ref. 8.

D. Virtual body

In this part of the experiment a series of runs with different magnet velocities and currents are performed to identify the regimes of the flow. Typical images of the flow are shown in Figs. 3 and 4. When the speed of the magnet is relatively large and the force is relatively weak, the wake behind the magnet is stable and is in the form of a jet [Fig. 3(a)] flowing in the direction of motion of the forcing. For larger values of J , the formation of a recirculation in the form of a vortex dipole [Fig. 3(b)] is observed under the magnet. The dipole does not remain stable however and starts shedding vortices. As the dipole loses vorticity of one sign it becomes asymmetric and eventually turns in the direction of rotation of the remaining vortex. This results in the formation of a typical Kármán-Bénard vortex street as shown in Fig. 4. When the forcing is increased even further, the nonlinearity of the flow increases to such an extent that the forcing produces strong compact vortex dipoles, which are ejected in different directions quasiperiodically without forming an organized vortex street. When the flow forms a regular vortex street, the wavelength of the street and the period of vortex shedding can be measured in the same manner as that described for the experiments with a cylinder.

III. DATA ANALYSIS

The wavelength of the vortex street, λ , is measured for the cylinder wakes and those generated by a virtual body. The frequency of the vortex shedding can then be introduced as $f=U/\lambda$ where U is the velocity of the body. In order to better understand the behavior of f for different values of the control parameters involved in the problem, it is useful to perform a simple dimensional analysis first. For the cylinder, the frequency f depends on a set of three dimensional quantities including kinematic viscosity ν , velocity U , and the diameter of the cylinder d . The dependence of frequency on the control parameters which must be determined in our experiments can be written in dimensionless form as

$$\text{Ro} = \Phi(\text{Re}), \quad (2)$$

where $\text{Ro}=fd^2/\nu$ is the so-called Roshko number³ and Φ is an unknown function of the Reynolds number $\text{Re}=dU/\nu$.

The Roshko number is a dimensionless measure of frequency while the Reynolds number characterizes the ratio of the nonlinearity to the dissipation in the flow. A number of experiments^{9,10} provide evidence for a linear dependence in the form

$$\text{Ro} = 0.212(\text{Re} - 21.2) \quad (3)$$

for moderate values of the Reynolds number in the range $\text{Re} = 50 - 180$. This dependence can be verified in our experiments.

For a virtual body, however, there is one additional dimensional parameter, namely the magnitude of the force J . Note that the force applied by the cylinder on the fluid is not an independent parameter but rather depends on the control parameters of the flow through the relation

$$J = C_D d U^2 / 2, \quad (4)$$

where C_D is the drag coefficient, which is dependent on the Reynolds number of the flow. The plot of C_D as a function of Re can be found in many textbooks on fluid dynamics (e.g., Ref. 11). When J is a free parameter, the dimensionless dependence can be written in the form

$$\text{Ro} = \Phi(\text{Re}, \Pi_d), \quad (5)$$

where an additional dimensionless parameter is $\Pi_d = J/(dU^2)$. In the experiments with a virtual body, two of the original dimensional parameters, namely U and J , can be varied (the diameter of the magnet is fixed) and the regimes of the flow can be observed. The diagram of regimes, where different symbols indicate the regimes (stable jet, vortex street, vortex dipole), can then be plotted in the space of dimensionless parameters Re and Π_d .

After this investigation of regimes is performed, it is desirable to simplify the problem and to reduce it to that for a circular cylinder. For this purpose the current in the apparatus can be adjusted so that the dependence of Eq. (4) is satisfied and the virtual body imitates a real cylinder. Note that the values of the Reynolds number should also be close to those used for the cylinder flow experiment. The dependence of Ro on Re can then be compared to that for the circular cylinder.

IV. CONCLUSION

We have presented a laboratory experiment to study the hydrodynamical phenomenon of periodic vortex shedding. The subject of this experiment is a complex (nonlinear) fluid flow; however the experiment does not require special knowledge of fluid dynamics. Rather, it involves general physical principles such as dimensional analysis and conservation laws. The method is based on an electromagnetic technique for generating the flows. This method is not routine, and although simple, is used in advanced research.

The experiment described in this paper can be easily simplified for use in an entry-level or intermediate undergraduate laboratory. In that case the students perform only the part where the cylinders are towed; they then compare their results with those of classical experiments.¹¹ Figure 5 shows the linear relationship between Roshko number and Reynolds number for cylinders of diameter 0.3–1.0 cm; for this case, the bottom layer of fluid consisted of salt water (250 g/l), while the upper layer was fresh water (we do not need to apply a current in this case).

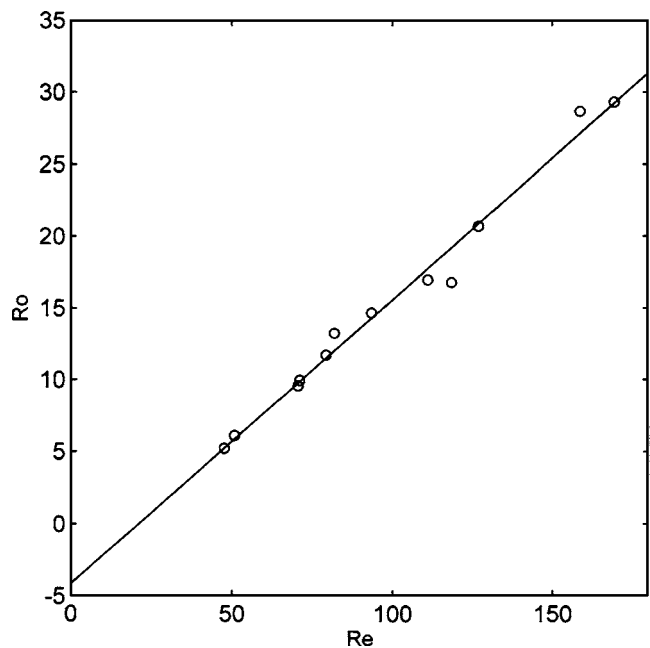


Fig. 5. Experimental results showing the linear relation between Roshko number and Reynolds number. A least squares fit to the data gives $\text{Ro} = 0.20(\text{Re} - 21)$ which is consistent with Eq. (3).

The experiment can also be modified for the more advanced level. Two magnets of opposite polarity can be used to imitate self-propelled objects such as swimming microorganisms, fish, or submarines. (Strictly speaking, only the laminar wakes with small or moderate values of the Reynolds number can be modeled using this setup.) Self-propelled bodies generate zero-momentum flow when moving with constant speed because they must transfer momentum to the fluid in the direction opposite to that of their motion to generate a thrust force. If a self-propelled body moves with constant speed, the drag and thrust forces are of equal magnitude and are in opposite directions. The drag force is applied near the front of the body while the thrust force is usually generated near the rear end. Thus, these forces are separated by a distance which is approximately equal to the length of the body. This same statement is also true for the corresponding reaction forces which act on the fluid. A rich variety of regimes of the flow can be observed in the experiments with two magnets. The experiment described in this paper can also include a PIV system,⁷ which would allow measurements of the velocity in the flows to be made. In particular, the profile of velocity in the wake behind a cylinder or a magnet can be measured, and the volume flux Q in the wake can be determined. This volume flux is directly related to the force applied by the body (real or virtual) via $J = UQ$.

ACKNOWLEDGMENTS

The research reported in this paper has been supported by the Natural Sciences and Engineering Research Council of Canada under Grants Nos. 300805-04 and 227192-04.

^{a)} Author to whom correspondence should be addressed. Electronic mail: yakov@physics.mun.ca

¹R. N. Govardhan and O. N. Ramesh, "A stroll down Kármán street," *Resonance* **10**, 25–37 (2005).

²G. K. Batchelor, *An Introduction to Fluid Dynamics* (Cambridge U. P., Cambridge, MA, 2000).

³M. M. Zdravkovich, *Flow Around Circular Cylinders* (Oxford U. P., Oxford, 1997).

⁴J. Paret, D. Marteau, O. Paireau, and P. Tabeling, "Are flows electromagnetically forced in thin stratified layers two dimensional?" *Phys. Fluids* **9**, 3102–3104 (1997).

⁵Electrochemical reactions will cause the copper electrodes to deteriorate and contaminate the fluid in the tank. To reduce this effect the electrodes can be wrapped in the filter paper. Better results can be obtained with graphite electrodes.

⁶Y. D. Afanasyev and V. N. Korabel, "Starting vortex dipoles in a viscous fluid: asymptotic theory, numerical simulations and laboratory experi-

ments," *Phys. Fluids* **16**, 3850–3858 (2004).

⁷Y. D. Afanasyev, "Investigating vortical dipolar flows using Particle Image Velocimetry: An experiment for an advanced undergraduate laboratory," *Am. J. Phys.* **70**, 86–88 (2002).

⁸F. Noca, D. Shiels, and D. Jeon, "A comparison of methods for evaluating time-dependent fluid dynamic forces on bodies, using only velocity fields and their derivatives," *J. Fluids Struct.* **13**, 551–578 (1999).

⁹A. Roshko, On the development of turbulent wakes from vortex streets, Ph.D. thesis, California Institute of Technology, 1952.

¹⁰D. J. Tritton, "Experiments on the flow past a circular cylinder at low Reynolds numbers," *J. Fluid Mech.* **6**, 547–567 (1959).

¹¹D. J. Tritton, *Physical Fluid Dynamics* (Oxford U. P., Oxford, 1988).

Inexpensive fabrication of silicon Hall devices

Jed Brody, Zhiyong Dong, and Tristan Dennen

Department of Physics, Emory University, Atlanta, Georgia 30322

(Received 3 January 2006; accepted 6 January 2006)

Semiconductor Hall devices are typically prefabricated for instructional laboratories, but students may gain more understanding by fabricating their own devices. Semiconductor device fabrication usually involves photolithography, vacuum evaporators, and very high-temperature tube furnaces. This paper presents an inexpensive procedure to fabricate silicon Hall devices using only a hot plate and indium. van der Pauw resistivity measurements of *p*-type and *n*-type samples thus fabricated yielded results well within the manufacturer's specifications. Hall measurements of these samples consistently indicated the correct carrier type in both cases. For both *p*-type and *n*-type samples, the carrier concentrations obtained from the Hall measurements were within 4% of the expected values. © 2006 American Association of Physics Teachers.

[DOI: 10.1119/1.2173275]

I. INTRODUCTION

The Hall effect is commonly investigated in instructional laboratories. Performing Hall measurements of both *p*-type and *n*-type semiconductors is especially instructive; however, semiconductor Hall devices are often prefabricated, and therefore students may lack a clear understanding of the geometry and the physics of the devices. Indeed, in their haste to collect data, students may take but a cursory glance at the devices before recording currents and voltages of mysterious origin. Students who fabricate their own Hall devices may better visualize the applied currents, magnetic fields, and resulting voltages. Additionally, gaining experience with processing semiconductor wafers is valuable in itself. The formation of ohmic contacts on semiconductors is not, however, a trivial task;¹ typically, semiconductor devices are fabricated using photolithography, evaporators, and very high-temperature tube furnaces. This paper presents an inexpensive procedure for fabricating silicon Hall devices using little more than indium and a hot plate.

The procedure described here was developed largely through trial and error. The suggestion to melt indium on a hot plate was made by Gregory Triplett of the Georgia Institute of Technology.

II. PROCEDURE

Hall devices were fabricated using float zone silicon wafers, one *p*-type and one *n*-type. The resistivities specified by

the manufacturer (SEH) were 2–2.7 Ω cm and 1–5 Ω cm, respectively. The measured thicknesses were 0.0295 cm and 0.0220 cm, respectively. A diamond-tipped scriber was used to cleave from each wafer an approximately rectangular sample measuring about 4–7 cm on each side. Each sample was processed as follows.

The first step was to remove the native oxide, which forms on silicon surfaces exposed to air. If not removed, the native oxide could be an insulating layer between the silicon and

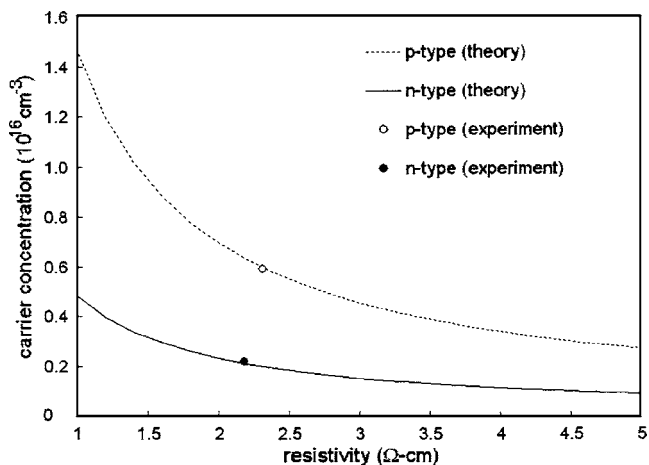


Fig. 1. Acceptable agreement between experiment and theory for both *p*-type and *n*-type Hall samples.

Table I. van der Pauw resistivity data and calculated resistances for the *p*-type silicon sample.

	Current	Voltage	Resistance
(1)	$I_{21}=2.044$ mA	$V_{34}=18.90$ mV	$R_{21,34}=9.247$ Ω
(2)	$I_{12}=2.044$ mA	$V_{43}=19.09$ mV	$R_{12,43}=9.340$ Ω
(3)	$I_{43}=2.044$ mA	$V_{12}=18.88$ mV	$R_{43,12}=9.237$ Ω
(4)	$I_{34}=2.044$ mA	$V_{21}=18.77$ mV	$R_{34,21}=9.183$ Ω
(5)	$I_{32}=2.044$ mA	$V_{41}=59.18$ mV	$R_{32,41}=28.95$ Ω
(6)	$I_{23}=2.044$ mA	$V_{14}=59.51$ mV	$R_{23,14}=29.11$ Ω
(7)	$I_{14}=2.044$ mA	$V_{23}=59.87$ mV	$R_{14,23}=29.29$ Ω
(8)	$I_{41}=2.044$ mA	$V_{32}=59.61$ mV	$R_{41,32}=29.16$ Ω

the metal contact. In an effort to remove the native oxide, Scotch tape was pressed onto the four corners of the sample and peeled off. Next, four thin slices of indium were sliced with a razor blade from a rod of 0.125 in. diameter. A slice of indium was pressed onto each corner of the sample. The sample was placed on a hot plate set above the melting point of indium (157 °C). The indium melted instantly.

The next step, discovered by accident, appears to improve the contact quality. Metal tweezers were dipped into the molten indium and gently scraped along the silicon-indium interface. Then the wafer continued sitting on the hot plate for about 3 minutes. After the wafer cooled, a thin wire (30 gauge) was placed on each indium contact. An additional indium slice was placed over each wire and pressed firmly to secure the wire.

Next, van der Pauw resistivity and Hall measurements were performed as described by NIST.² According to this procedure, the four contacts were designated 1, 2, 3, and 4 in counterclockwise order. Currents and voltages are specified by pairs of subscripts. The current I_{21} , for example, indicates a positive current flowing into 2 and out of 1. The voltage V_{34} indicates the voltage at 3 minus the voltage at 4. Then $R_{21,34}$ is defined as V_{34}/I_{21} . Voltage measurements in the presence of a magnetic field are indicated by adding “*P*” or “*N*” to the subscripts; “*P*” represents a magnetic field pointing out of the top of the sample, and “*N*” represents a magnetic field in the opposite direction. All currents were supplied by an op amp current source³ (students who have studied op amps may apply their skills by building the current source themselves). The magnetic field was produced by an electromagnet, and a gaussmeter was used to measure the magnetic field.

III. RESULTS

Tables I and II show currents and voltages measured during the van der Pauw resistivity experiment for both silicon samples; the resistances were calculated from the measured currents and voltages. The data are organized by pairs of reversed polarity for both current and voltage. In all cases, the resistance values obtained by polarity reversal are within 3% of each other. This indicates adequate measurement consistency.

The van der Pauw measurements yield two characteristic resistances: one is the average of the first four resistances given in the table, and the other is the average of the final four. For the *p*-type sample, the characteristic resistances obtained are 9.263 Ω and 29.13 Ω . For the *n*-type sample, the characteristic resistances are 9.325 Ω and 43.09 Ω .

The Hall effect is clearly observed in Tables III and IV. For the *p*-type sample, the voltages in the positive magnetic field are about 2.2 mV higher than those in the negative magnetic field. For the *n*-type sample, the voltages in the positive field are about 5.8 mV lower than those in the negative field. Thus the correct carrier types are clearly and consistently indicated.

IV. ANALYSIS AND DISCUSSION

By using the two characteristic resistances found in Table I and solving the van der Pauw equation,² the sheet resistance of the *p*-type sample is found to be 78.26 Ω . From this, the resistivity is calculated as 2.31 Ω cm, in good agreement

Table II. van der Pauw resistivity data and calculated resistances for the *n*-type silicon sample.

	Current	Voltage	Resistance
(1)	$I_{21}=1.500$ mA	$V_{34}=13.98$ mV	$R_{21,34}=9.320$ Ω
(2)	$I_{12}=1.500$ mA	$V_{43}=14.03$ mV	$R_{12,43}=9.353$ Ω
(3)	$I_{43}=1.500$ mA	$V_{12}=14.12$ mV	$R_{43,12}=9.413$ Ω
(4)	$I_{34}=1.500$ mA	$V_{21}=13.82$ mV	$R_{34,21}=9.213$ Ω
(5)	$I_{32}=1.500$ mA	$V_{41}=64.81$ mV	$R_{32,41}=43.21$ Ω
(6)	$I_{23}=1.500$ mA	$V_{14}=64.49$ mV	$R_{23,14}=42.99$ Ω
(7)	$I_{14}=1.500$ mA	$V_{23}=64.83$ mV	$R_{14,23}=43.22$ Ω
(8)	$I_{41}=1.500$ mA	$V_{32}=64.41$ mV	$R_{41,32}=42.94$ Ω

Table III. Hall measurements for the p -type sample in a magnetic field of ± 1500 G.

$I_{13}=2.044$ mA	$V_{24P}=41.99$ mV
$I_{31}=2.044$ mA	$V_{42P}=41.89$ mV
$I_{42}=2.044$ mA	$V_{13P}=-38.96$ mV
$I_{24}=2.044$ mA	$V_{31P}=-39.76$ mV
$I_{13}=2.044$ mA	$V_{24N}=39.80$ mV
$I_{31}=2.044$ mA	$V_{42N}=39.70$ mV
$I_{42}=2.044$ mA	$V_{13N}=-41.20$ mV
$I_{24}=2.044$ mA	$V_{31N}=-41.95$ mV

with the manufacturer's specifications of 2–2.7 Ω cm. For the n -type sample, the sheet resistance obtained is 99.24 Ω and the resistivity is 2.18 Ω cm, well within the manufacturer's designation of 1–5 Ω cm.

The Hall measurements in Tables III and IV can be used to determine carrier concentrations.² The carrier concentration of the p -type sample is found to be 5.92×10^{15} cm⁻³. This is within 2% of the expected concentration⁴ for a p -type sample with the resistivity found above. The carrier concentration of the n -type sample is obtained as 2.19×10^{15} cm⁻³. This is within 4% of the expected concentration⁴ for an n -type sample with the resistivity found above. A graphical comparison of experiment and theory is given in Fig. 1. The difference between p -type and n -type silicon is striking and confirmed by our measurements.

The results reported here are for samples with resistivities near 2 Ω cm, and the agreement between experimental results and theory is very good. Additional work is needed to determine the range of silicon resistivities for which indium contacts are appropriate. Our previous attempts with 0.6 Ω cm p -type silicon failed to produce a good sample. We expect, however, that our good results near 2 Ω cm may be reproduced in other instructional laboratories.

Table IV. Hall measurements for the n -type sample in a magnetic field of ± 1500 G.

$I_{13}=1.500$ mA	$V_{24P}=47.39$ mV
$I_{31}=1.500$ mA	$V_{42P}=48.09$ mV
$I_{42}=1.500$ mA	$V_{13P}=-53.40$ mV
$I_{24}=1.500$ mA	$V_{31P}=-53.78$ mV
$I_{13}=1.500$ mA	$V_{24N}=53.35$ mV
$I_{31}=1.500$ mA	$V_{42N}=53.92$ mV
$I_{42}=1.500$ mA	$V_{13N}=-47.56$ mV
$I_{24}=1.500$ mA	$V_{31N}=-48.04$ mV

V. CONCLUSIONS

Metal contacts were formed on p -type and n -type silicon samples by melting indium with a hot plate. van der Pauw resistivity measurements on these samples yielded results that fell well within the manufacturer's specifications of 2–2.7 Ω cm for the p -type sample and 1–5 Ω cm for the n -type sample. Hall measurements correctly indicated carrier type in both samples. The Hall measurements also yielded carrier concentrations within 4% of the expected values. The simple, inexpensive procedure described in this paper produces good Hall samples and can be performed easily by students.

¹Kevin F. Brennan, *The Physics of Semiconductors* (Cambridge U. P., New York, 1999), p. 567.

²Excellent and thorough instructions for van der Pauw resistivity and Hall measurements are available at <http://www.eeel.nist.gov/812/hall.html>

³Thomas C. Hayes and Paul Horowitz, *Student Manual for the Art of Electronics* (Cambridge U. P., New York, 1989), p. 180.

⁴A carrier concentration calculator is available at <http://www.solecon.com/sra/rho2ccal.htm>